Heat transfer characteristics and flow visualization during flow boiling of acetone in semi-open multi-microchannels

XIA, Guodong, CHENG, Yue, CHENG, Lixin and LI, Yifan

Published version

XIA, Guodong, CHENG, Yue, CHENG, Lixin and LI, Yifan (2018). Heat transfer characteristics and flow visualization during flow boiling of acetone in semi-open multi-microchannels. Heat Transfer Engineering, 1-14.

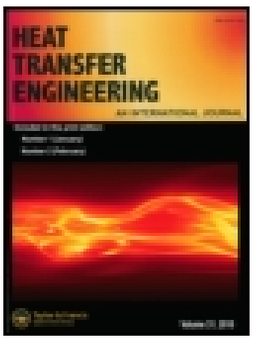

Heat Transfer Engineering

ISSN: 0145-7632 (Print) 1521-0537 (Online) Journal homepage: http://www.tandfonline.com/loi/uhte20

Heat Transfer Characteristics and Flow Visualization during Flow Boiling of Acetone in Semi-open Multi-microchannels

Guodong Xia, Yue Cheng, Lixin Cheng & Yifan Li

To cite this article: Guodong Xia, Yue Cheng, Lixin Cheng & Yifan Li (2018): Heat Transfer Characteristics and Flow Visualization during Flow Boiling of Acetone in Semi-open Multi-microchannels, Heat Transfer Engineering, DOI: 10.1080/01457632.2018.1470296

To link to this article: https://doi.org/10.1080/01457632.2018.1470296

Accepted author version posted online: 30 Apr 2018.

Publisher: Taylor & Francis

Journal: *Heat Transfer Engineering*

DOI: https://doi.org/10.1080/01457632.2018.1470296

Heat Transfer Characteristics and Flow Visualization during Flow Boiling of Acetone in Semi-open Multi-microchannels

GUODONG XIA[a], **YUE CHENG**[a], **LIXIN CHENG**[a,b], and **YIFAN LI**[a]

[a]College of Environmental and Energy Engineering, Beijing University of Technology, Chaoyang, Beijing, China

[b]Department of Engineering and Mathematics, Sheffield Hallam University, City Campus, Sheffield, UK

Address correspondence to Professor Guodong Xia, College of Environmental and Energy Engineering, Beijing University of Technology, Chaoyang, Beijing 100124, China. E-mail: xgd@bjut.edu.cn

Abstract

Experimental results of flow boiling characteristics and flow patterns with acetone in two different microchannel heat sinks are presented in this paper. A semi-open microchannel heat sink and a straight microchannel heat sink with 19 parallel microchannels each were designed and tested. The semi-open microchannels have a channel width of 0.8 mm, fin width of 0.4 mm and pedestal height of 0.2 mm and the straight microchannels have a rectangular cross section of 0.8 mm×1 mm. The experimental heat fluxes ranged from 0 to 90 kW/m^2, vapor quality ranged from 0.05 to 0.5, mass fluxes ranged from 4.34 to 15.62 kg/m^2·s and the inlet temperatures were

20 and 30 °C respectively. Compared to those in the straight microchannels, flow boiling heat transfer coefficients can be improved by up to 36.2%. Furthermore, flow patternss were observed with a speed video camera. The flow boiling heat transfer mechanisms are analyzed according to the observed flow patterns.

NOMENCLATURE

A_{ch} total heat area of microchannels, m^2

c_p specific heat of acetone, J/kgK

CHF critical heat flux, W/m^2

G mass flux, kg/m^2s

h_{fg} latent heat of vaporization, kJ/kg

h_{tp} local two-phase heat transfer coefficient, kW/m^2K

H height, m

I the voltage and current, A

k thermal conductivity, W/m·k

L length of heat sink, mm

L_i distance from the inlet to thermocouple location in the downstream direction, m

m fin parameter

$\dot{m}$ the mass flow rate, kg/s

N number of electrical cartridge heaters

ONB onset of nucleation boiling

P_{in} pressure of inlet, Pa

P_{out} pressure of outlet, Pa

q_{in} total power input, W

q_{eff} effective absorbed heat,W

q''_{eff} effective heat flux based on platform area, kW/m^2

R thermal resistance, °C /W

T_{tci} thermocouple reading, °C

T_{in} inlet fluid temperature, °C

T_{out} outlet fluid temperature, °C

$T_{\text{w, tci}}$ channel bottom wall temperature at thermocouple location, °C

$\Delta T_{\text{sct,tci}}$ wall superheat, °C

$T_{\text{sat,tci}}$ local saturation temperature of thermocouple location, °C

T_{in} inlet fluid temperature, °C

U voltage, V

W width, m

w_c width of channel, m

x thermodynamic vapor quality

Greek symbols

δ width of fin, m

η fin efficiency

λ thermal conductivity, W/mK

φ the heat transfer ratio

Subscripts

Cu copper

cell unit cell of channel

cp cover plate

fin fin

tci thermocouple location

in inlet

out outlet

sat saturation

tp two-phase

c channel

l1 channel length of closed section

l2 channel length of open section

INTRODUCTION

With the rapid development of modern science and technology, flow boiling and two-phase flow in micro- and mini-channels play a significant role in cooling high heat flux in various engineering applications. Over the past decades, VLSI (vast large scale integrated) chips' heat fluxes have already reached up to 300 W/cm^2. The traditional cooling technology cannot meet the growing demand of heat dissipation in microelectronics and high-performance computer chips etc. Tuckerman and Pease [1] investigated heat transfer performance in microchannel heat sinks which have potential ability in electronic cooling. Mudawar [2] investigated flow boiling heat transfer in mini-channels and microchannels for high heat flux thermal management application. According to the existing studies, flow boiling in micro- and mini-channel heat sinks may provide high heat transfer rates and stable wall

temperature control. Therefore, a number of researchers have investigated flow boiling heat transfer and two-phase flow in micro- and mini-channels in multiple systems over the past decades [3-18]. This topic is still a “hottest” research area due to the very complicated phenomena and mechanisms involved in various channels. It is worth to conduct the relevant experimental and theoretical research on the relevant topics as pointed by Cheng and Xia [19].

Kandlikar et al. [3] reported that the inverse flow (bubbles expand against the current) was observed in parallel rectangle mini-channels with a hydraulic diameter of 1 mm by using high speed camera. Steinke and Kandlikar [4] investigated the flow boiling pheromone of water in 6 parallel microchannels with a hydraulic diameter of 207 μm. The results of visualization showed that the cause of inverse flow is a rapid increase of bubbles. Qu and Mudawar [5] researched that the max flow boiling heat transfer coefficient is 130 W/cm^2 for the 21 parallel microchannels with a rectangular cross section of 231 μm × 713 μm.

More recently, Shah [6] researched a new correlation for flow boiling both in macro and mini/micro channels using 4852 experimental heat transfer data points from 137 data sets from 81 study sources. The database contains experimental data with 30 different fluids, including water, CO_2, ammonia, halocarbon refrigerants, organics and cryogens etc., the hydraulic diameters of the microchannels ranges from 0.38 to 27.1 mm, different channel shapes (round, rectangle, triangle), fully or partially heated, horizontal and vertical downflow. The test conditions of the database

cover the mass flux from 15 to 2437 kg/m^{2}s, the reduced pressure from 0.0046 to 0.787. The mean absolute deviation for all data points is 18.6 %, lower than other heat transfer correlations in the literature. In addition, his study indicates that the function of Weber number and boiling number which is given by the new correlation both influence the border between macro-channels and mini-channels for flow boiling. Therefore, it is unreasonable that the classification of macro-channels and mini-channels just base on diameter or Bond number.

Cheng and Xia [19] have presented a comprehensive review on the fundamental issues, mechanisms and models of flow boiling heat transfer in micro-channels. They compared several existing models and correlations and found that none of the exiting models can predict the whole database. They have pointed out that it is essential to further develop generalized mechanistic flow boiling heat transfer models.

Huang and Thome [7] proposed a new multi-microchannel evaporator and a novel flow pattern-based model for local heat transfer prediction. R245fa and R236fa were tested in the new evaporator at three different outlet saturation temperatures. The experimental results showed that the heat transfer performance decreased at the single-phase thermal developing flow and then increased at the onset of saturated flow boiling, and finally it decreased again when the flow regime go into the annular flow pattern. The new flow pattern-based model uses 1,941,538 data points and the mean absolute deviation for all data points is 14.2% and 90.1% of the data predict within

±30%. This is very promising. It is suggested to verify the model with extensive experimental data with various working fluids.

Cheng [8] conducted a comprehensive literature review on the critical heat flux (CHF) in microchannels and confined spaces. Quite different results and mechanisms are reported by various researchers. Furthermore, CHF of flow boiling (subcooled flow boiling and saturated flow boiling) in microchannels with various prediction methods are analyzed and discussed. CHF of nucleate pool boiling in confined spaces with prediction methods also are reviewed and discussed. He has indicated that flow regimes, flow instabilities, axial conduction, channel shape and number, heated length, fluid type, aspect ratio effect, the length-to-diameter ratio, and liquid film affect CHF and physical mechanisms should be considered in developing new models for CHF phenomena in micro-channels.

Wu and Cheng [9] conducted a series of experiments of flow boiling in trapezoidal microchannels within the specific limits of mass flux and heat flux. And indicated that there are three instable models: (1) Single-phase flow (liquid) and two-phase flow alternate appearance at low heat flux and high mass flux; (2) Continuous two-phase flow can be observed at middle heat and mass flux and (3) Two-phase flow and single-phase flow (vapor) alternate appearance at high heat flux and low mass flux. Hetsroni et al. [10] conduced experimental study of flow boiling in a parallel triangular microchannel heat sink and observed a good temperature uniformity, because the temperature difference on the surface is about 4-5°C. Chen et

al. [11] studied the heat transfer performance of subcooled flow boiling in narrow annular (1 mm and 2 mm). They concluded that the flow boiling has palpable hysteresis quality in narrow annular, and the heat transfer coefficient of 1 mm narrow annular is almost 40% higher than the heat transfer coefficient of 2 mm narrow annular. In the same heat transfer coefficient, pressure drop and mass flux of 1 mm narrow annular are smaller than 2 mm narrow annular. Zhang et al. [12] established 3-D steady heat transfer model of constant wall temperature of fractal tree-like microchannel nets on the basis of the Chen and Cheng [13] scheme, which is constructal tree-shaped minichannel network. Their numerical solution showed that the heat effective coefficient and pressure drop of the network is better than the serpentine channel.

Wu and Cheng [14, 15] reported the flow boiling pheromone of water of parallel silicon microchannels of trapezoidal cross-section. The wall temperature, working substance temperatures, pressures and mass flux were researched in a series of experiments, and flow regimes such as bubbly flow, slug flow, churn flow were observed. Wang et al. [16] investigated the flow boiling performance of widening mini-channels of U-shaped section. The critical heat flux is 27 W/cm^2 which is double of the critical heat flux of straight mini-channels. Yang et al. [17] studied the flow boiling heat transfer with inlet restrictors. The heat transfer coefficient is almost 149% higher than the straight channels, and pressure drop is almost 71% lower than the straight channels. The range of mass flux is from 400 $kg/m^2 \cdot s$ to 1400 $kg/m^2 \cdot s$, and

the critical heat flux is 552 W/cm^2 when mass flux is 480 kg/m^2·s. Kandlikar et al. [18] used an over open microchannels. It has higher heat transfer coefficient and critical heat flux than other forms of channels, and pressure drop is less than 10 kPa.

In the present study, experiments of flow boiling heat transfer characteristics were conducted a semi-open microchannel heat sink and a straight microchannel heat sink. The experimental results were compared with each other. The influences of heat flux, vapor quality, mass flux, inlet temperature, channel type, flow pattern, and instability on the flow boiling heat transfer coefficients are analyzed and discussed. Furthermore, flow patterns were observed with a high-speed video camera. The flow regimes in both microchannels were compared and analyzed. The observed flow regimes may be used in understanding the flow boiling mechanisms in the microchannel heat sinks.

EXPERIMENTAL RIG AND TEST SECTIONS

Experimental Setup

Fig. 1. shows the schematic of the experimental loop in the present study. The experimental loop mainly consists of a liquid tank together with a heater and vacuum pump, a gear pump, a flow meter, a preheater, a test section, a condenser, a bypass, pipe systems and an instrumentation system. The working fluid is acetone. Table 1 shows the comparison of the physical properties of acetone and water at 101.325 kPa [20]. The working fluid is pumped from a liquid tank by a gear pump (SERVECALL

L22570). The liquid tank has a capacity of 5.5 liter, and an immersion coil pipe heater is installed in the liquid tank, which is utilized to degas the non-condensable gas in acetone. The working fluid passes through a 30μm filter and then the flow rate is measured by a flowmeter (DMF-1-1A). Before the acetone entering the test section, the flowing is preheated by a constant temperature bath to obtain a stable subcooling temperature for the experiments, and then passes through a 2-5μm filter. The test sections are two microchannel heat sinks which are heated by electricity to generate flow boiling conditions. In the test section, there is a direct current power supply (ranged 0-50 V) which can display voltage and current concurrently. The heating power may be adjusted to obtain the desired test conditions of flow boiling in the test section. Then, fluid flows into the condenser and is condensed and the condensed fluid flows back to the liquid tank.

The measured parameters are flow rate, heating power, fluid inlet and out let temperatures and inlet and outlet pressures. The flow rate is measured with the flowmeter and the electrical heating power is measured with the voltage and electrical current. The temperatures are measured with thermocouples and the pressures are measured with pressure transducers. The measured parameters such as fluid inlet and outlet temperatures and pressures and wall temperatures are acquired by an oscillography (YOKOGAWA DL850). Flow visualizations are accomplished with a high-speed camera (Motion Pro X4) and an AF Nikkor 50mm f/1.8D lens. Light source is provided by a 120W LED focus lamp. The picture may be taken at

1000-11000 frames per second. The flow regime pictures and the measured data of flow boiling in the microchannel heat sinks may be synchronized by a synchronizer, then transported to computer. The measured data are stored in the computer for further reduction.

Configuration of Microchannel Heat Sinks

The microchannels structure with 3D model of two different types are showed in Fig. 2. Both types consist of nineteen parallel channels in the 25 mm × 25 mm heat region. The first type, the straight microchannels, as showed in Fig. 2(a), has a rectangular cross section of 0.8 mm×1 mm, as control group. The second type, the semi-open microchannels as showed in Fig. 2(b), has a channel width of 0.8 mm, fin width of 0.4 mm, pedestal height of 0.2 mm. The first half of the microchannels are closed just like the straight microchannels. The height of channels is 1mm. The second half of the microchannels are fabricated by lowering the fins' height by 0.2 mm and open channels.

Test Section

As shown in Fig. 3 (a), the test section consists of a steel plate, a Pyrex7740 glass top cover, one-piece microchannels copper heating block, a bottom housing, an O-ring, electrical cartridge heaters, silicone gaskets and an insulating base. Microchannels are incised on the oxygen-free copper heating block to greatly reduce the contact thermal resistance. Below the top surface of the heating block, there are

three horizontal holes that are equally ranged up in order of distance. The K-type thermocouples (TJ60-CAXL-032U-4) are implanted in the holes to measure the temperature of the microchannels for places. Three other K-type thermocouples are vertical, equally spaced, and are used to evaluate the heat flux. The heating block exist a lug that can fix the copper block and the bottom housing to prevent displacement. Silicone rubber is used in the gap between the heating block and bottom housing to guarantee of a good seal. Four electrical cartridge heaters are housed in the bottom holes of the copper heating block to provide stable heat flux.

As shown in Fig. 3(b), the inlet and the outlet are arranged horizontally for working fluid. The inlet and the outlet are connected with a stainless steel tube to reduce the instability of flow. At the end-piece of the inlet, there is a rectangular sink which is implemented to drop the flow fluctuation of the incoming flow, and the side walls of the sink are designed two holes that are used to measure the pressures and the temperature respectively. The equalization board is set up at the top of the sink, to ensure that the working fluid is distributed in microchannels equably. The O-ring is pressed out between the glass top cover and bottom housing to seal up the working fluid. The bottom housing and the insulating base made of Teflon are used to insulate the copper heating block. When the all parts are mounted. the silicone gaskets and the steel plate can make sure the glass top cover won’t be cracked by the pressure.

DATA REDUCTION

In the single-phase flow, the effective heat absorbed by the acetone is determined by

$$q_{\text{eff}} = \dot{m} c_{\text{p}} (T_{\text{out}} - T_{\text{in}}) \quad (1)$$

where c_{p} is the specific heat of acetone (J/kg·K), $\dot{m}$ is the mass flow rate (kg/s). The total power input q_{in} is obtained straightly from the test：

$$q_{\text{in}} = N \times U \times I \quad (2)$$

N denotes the number of electrical cartridge heaters (4 electrical cartridge heaters used in this study). U and I respectively denotes the voltage and current, which are showed in the direct current power supply. Combining with the equations (1) and (2), the heat transfer ratio (φ), of which the effective heat absorbed by the acetone to the total power input can be obtained.

$$\varphi = \frac{q_{\text{eff}}}{q_{\text{in}}} \quad (3)$$

In the experiment of single-phase flow, the ratio (φ) is from 0.87 to 0.9, depending on the heat flux, inlet temperature, and mass flow in the experiments. The approximation of a linear dependency between q_{eff} (single-phase) and q_{in} (single-phase) leads to satisfactory results, so it is feasible to use the single-phase flow ratio value in the flow boiling experiments to obtain the absorbed heat.

One dimensional heat conduction equation, the temperature of the channel's bottom was calculated from thermal couple $T_{\mathrm{tci.}}$ The schematic of heat transfer cell was showed in Fig. 4. The wall temperature is given as follows:

$$T_{\mathrm{w,tci}} = T_{\mathrm{tci}} - \frac{q_{\mathrm{eff}} H_{\mathrm{cu}}}{k_{\mathrm{cu}}} \quad (4)$$

The effective heat flux q''_{eff} is calculated based on the effective area as

$$q''_{\mathrm{eff}} = \frac{q_{\mathrm{eff}}}{A_{\mathrm{ch}}} \quad (5)$$

where A_{ch} denotes the total effective area for convection in the straight microchannels shown in Fig. 4(a) and for the convection in the semi-open microchannels shown in Fig. 4(b), which are respectively given by Eqs. (6a) and (6b):

$$A_{\mathrm{ch}} = NL(w_{\mathrm{c}} + 2\eta_1 H_{\mathrm{l1}}) \quad \text{for the straight microchannel} \quad (6a)$$

$$A_{\mathrm{ch}} = NL(w_c + \eta_1 H_{\mathrm{l1}} + \eta_2 H'_{\mathrm{l2}}) \quad \text{for the semi-open microchannels} \quad (6b)$$

$$H'_{\mathrm{l2}} = H_{\mathrm{l2}} + \frac{\delta}{2} \quad (7)$$

where w_c is the perimeter of the width of the micro-channel, N is the total number of the semi-open microchannels, δ is the width of fin, η_1 represent an adiabatic fin tip condition which is used due to the non-conductive material of the top cover, for the l_1 (the channel of the first 12.5 millimeters), and η_2 represent a convective fin tip condition which is used for the l_2 (the channel of the last 12.5 millimeters) because of

the fin tip of stepped fin exposed to fluid flow. The fin efficiencies are given by Eqs. (8) and (9) as follows:

$$\eta_1 = \frac{\tanh(mH_{l1})}{mH_{l1}} \quad (8)$$

$$\eta_2 = \frac{\tanh(mH'_{12})}{mH'_{l2}} \quad (9)$$

where m is the fin parameter as calculated as follows:

$$m = \sqrt{\frac{h_{tp,tci}\ 2(L+\delta)}{\lambda L\delta}} \quad (10)$$

$$h_{tp,tci} = \frac{q_{eff}}{\Delta T_{sat,tci} A_{ch}} \quad (11)$$

the A_{ch} and $h_{tp,tci}$ can be calculated from Eqs. (6a), 6(b), (8), (9), (10) and (11) with an iterative scheme.

$$\Delta T_{sat,tci} = T_{w,tci} - T_{sat,tci} \quad (12)$$

where $\Delta T_{sat,tci}$ is the local wall superheat degree, $T_{w,tci}$ is the local wall tempera -ture and $T_{sat,tci}$ is the local saturation temperature based on the local pressure. Linear distribution of pressure drop along the stream-wise direction is assumed. The vapor quality is defined as an energy balance as follow,

$$x = \frac{1}{h_{fg}}[\frac{q_{eff}}{\dot{m}}\frac{L_i}{L}\ \ c_p(T_{sat,tci} - T_{in})] \quad (13)$$

Where h_{fg} is the latent heat of vaporization, L_i is the distance from the measuring location to the inlet, c_p is constant-pressure specific heat. In the present study, the local boiling heat transfer of the downstream thermal couple position (T_{tc3}) which is near the outlet of channel was paid close attention.

Measurement Uncertainties

Using a standard error analysis [21], the measurement of uncertainties for the experimental parameters are summarized in Table 2. The following equations are used to analyze the uncertainties:

$$\frac{\Delta q_{eff}}{q_{eff}} = \sqrt{(\frac{\Delta \dot{m}}{\dot{m}})^2 + (\frac{\Delta \delta T}{\delta T})^2} \quad (14)$$

$$\frac{\Delta h_{tp,tci}}{h_{tp,tci}} = \sqrt{(\frac{\Delta q_{eff}}{q_{eff}})^2 + (\frac{\Delta A_{ch}}{A_{ch}})^2 + (\frac{\Delta \delta T}{\delta T})^2} \quad (15)$$

$$\frac{\Delta x}{x} = \sqrt{(\frac{\Delta q_{eff}}{q_{eff}})^2 + (\frac{\Delta A_{ch}}{A_{ch}})^2 + (\frac{\Delta \delta T}{\delta T})^2 + (\frac{\Delta L}{L})^2} \quad (16)$$

EXPERIMENTAL RESULTS AND DISCUSSION

Boiling Curves

Boiling curves were plotted for the straight micro-channel sink and semi-open micro-channel sink at different mass fluxes in Figs. 5 and 6, respectively. The boiling curves show the effective heat fluxes versus the local wall superheat (the temperature

difference between the wall and the local saturation temperature) obtained from the end of the channel near the outlet (T_{tc3}). Six mass fluxes from 4.34 kg/m^{2}s to 15.62 kg/m^{2}s for the heat fluxes in the range of 0-90 kW/m^2 are illustrated in the boiling curves. The inlet temperature of the acetone was controlled at 20°C, which meant the subcooling of boiling curves was approximate 36°C in the present study. According the boiling curves, with increasing heat flux, the temperature of wall rapidly rises. A single-phase forced convection in channel may be observed in the beginning. When the heat transfer processes reach the onset of nucleate boiling (ONB), the slopes of the boiling curves abruptly change. It also shows that the higher mass flow rate lead to a larger heat flux at a given wall superheat, no matter in the single-phase region or the boiling region in both types of microchannels. It shows that the heat flux of ONB depends on the mass flux. Higher heat fluxes may occur at ONB with increasing the mass flux in both types of microchannels as shown in Figs 5 and 6. This is in consistent with the results reported by Galvis and Culham [22]. In addition, the semi-open microchannels are able to touch off the ONB at a smaller wall temperature overshoot than straight microchannels at the same mass flux. The minimum temperature overshot of semi-open microchannels is 1.3℃, which is smaller than other pass studied by Sun et al. [23]. It may be attributed to that the semi-open microchannels provide more active nucleate sites, promoting bubble embryos to grow and depart at low wall temperature overshoot. By the same token, wall superheat excursion found after the initiation of boiling in semi-open microchannels is smaller

than it in straight one. After the ONB, the boiling curves at different mass fluxes have the same starting point. This may be relevant to the nucleate boiling dominant region. With further increasing the heat fluxes, the boiling curves at different mass fluxes separate, implying that heat fluxes are strongly dependent on the mass fluxes.

As shown in Fig. 5, the curves coincide with each other at above 5℃ of superheat for high mass flow rates (G =13.02 -15.62 kg/m^2 s). It is notable that the mass fluxes have little effect on the boiling curves after the temperature overshoot, illustrating that the nucleate boiling mechanism is the dominance in the straight microchannels. However, for the semi-open microchannels, the curves are separated from each other as showed in Fig. 6, implying that the convective boiling mechanism dominates over the nucleate boiling mechanism. These observations are in consistent with the phenomena observed by Galvis and Culham [22].

The Effects of Heat Flux on Flow Boiling Heat Transfer

The effects of heat flux and vapor quality on the local heat transfer coefficients are illustrated in Figs. 7 and 8. In all cases, the local heat transfer coefficients reach the maximum at the starting point of boiling. The number of nucleation sites may be provided for numerous tiny cavities existing in the wall of semi-open microchannels. The nucleation sites lead to the bubble formation, up-growth and departure when the nucleate boiling begins. The phenomenon caused massive release of latent heat to the outside, so the h_{tp} in all cases was large at the initial region of boiling. The stage had

something to do with the nucleate boiling dominant region [24]. It can be more obviously showed in Fig. 7 that the heat coefficients for all mass fluxes converge into a single set of curves at the initial region of boiling, indicating that the mass flux had weak influence on the flow boiling heat transfer coefficients [25, 26]. With increasing the heat flux and vapor quality, the flow boiling heat transfer coefficients decreases at low mass fluxes. These results are also reported by Sumith et al. [27]. This observation may be explained by the forced connective boiling dominant heat transfer mechanisms. According to the observed flow regimes related to the heat transfer behaviors, both the churn flow and annular flow regimes occur in the microchannels, and the heat transfer is mainly through the thin film evaporation. Due to these contributions based on the observed flow regimes and heat transfer mechanisms, the forced convective boiling heat transfer dominates in the boiling process at these conditions. The heat flux and vapor quality have a significant effect on the flow boiling heat transfer performance in the semi-open microchannels.

The Effects of Mass Flux on Flow Boiling Heat Transfer

The experimental include six different mass fluxes ranging from 4.34 kg/m^{2}s to 15.62 kg/m^{2}s and the inlet temperature was 20ºC as shown in Figs. 7 and 8. It can be seen that the flow boiling heat transfer coefficients have three different modes at diverse mass flux regions. In the low mass flux region of 4.34 kg/m^{2}s to 8.68 kg/m^{2}s, apart from the ONB region, the boiling process is dominated by forced connective boiling mechanism. With increasing the heat flux, the liquid film may become

thinner, which made bubbles to tend to not grow in the churn flow or annular flow. Furthermore, the dry-out phenomenon would happen more frequently. All these result in a decrease in the local heat transfer coefficient at low mass fluxes [28]. In the middle mass flux region of 11.28 kg/m^{2}s to 13.12 kg/m^{2}s, the local heat transfer coefficients become constant with increasing the heat flux until dry-out. The heat transfer process is dominated by the mixture boiling mechanisms including both the nucleate boiling dominated mechanism and forced connective boiling dominated mechanism [29]. In the high mass flux region of 15.62 kg/m^{2}s and above, the nucleate boiling mechanism controls the flow boiling heat transfer process in the microchannel. The local heat transfer coefficient stably increases with the increasing the heat flux. The high speed visualizations indicated that bubbly flow is the major visible flow patterns under the test condition. This heat transfer behavior was also observed by Bao et al. [30].

The Effects of Inlet Temperature on Flow Boiling Heat Transfer

Experiments were also conducted in the semi-open microchannels at two different inlet temperatures in order to research the effects of the inlet temperature on the flow boiling heat transfer performance. Two different inlet temperatures of 20ºC and 30ºC and three different mass fluxes of 6.94 kg/m^{2}s, 11.28 kg/m^{2}s and 15.62 kg/m^{2}s were used in the experiments. As seen in Figs. 9 and 10, for the inlet temperature of 20ºC, the highest heat transfer cofficient is 5524.18 W/Km^2 at the effective heat flux q''_{eff} = 27.36 kW/m^2 and a mass flux of 15.62 kg/m^{2}s. The lowest

heat transfer cofficient is 820.44 W/Km^2 at an effective heat flux q''_{eff} = 58.85 kW/m^2 and a mass flux of 6.94 kg/m^{2}s. The dry-out phenomenon occurs at the mass flux of 6.94 kg/m^{2}s. For the inlet temperature of 30ºC, the maximum heat transfer cofficient is 5134.16 W/Km^2 at an effective heat flux q''_{eff} = 22.49 kW/m^2 and a mass flux of 15.62 kg/m^{2}s. The lowest heat transfer cofficient is 736.97 W/Km^2 at an effective heat flux q''_{eff} = 54.14 kW/m^2 at a mass flux of 6.94 kg/m^{2}s. From the measured results shown in Figs. 9 and 10, the inlet temperature has a significant effect on the flow boiling heat transfer behavior. The heat transfer coefficients at the low inlet temperature of 20ºC are higher than those at the high inlet temperature of 30ºC in the range of mass fluxes used. The phenomena are mainly due to the liquid of low inlet temperature could absorbs more heat and main better heat transfer performance.

The Effects of the Microchannel Types on Flow Boiling Heat Transfer

As shown in Figs. 11 and 12, the semi-open microchannels have a better heat transfer performance than the straight microchannels at low or middle mass fluxes. This is involved with its larger surface area and thus results in more nucleation sites in the boiling process. It shows that the straight microchannels have lower flow boiling heat transfer coefficients than the semi-open microchannels at low or middle mass fluxes while both microchannels have similar heat transfer coefficients at high mass fluxes. With increasing the heat fluxes and vapor qualities, both type of microchannels show similar variations of heat transfer coefficients. At high mass fluxes, the flow boiling heat transfer coefficient increases with increasing the mass

flux except the onset of nucleate boiling. At middle mass fluxes, flow boiling heat transfer coefficients keep constant and the heat flux and vapor quality have little effects on the results. At low mass fluxes, both the types of microchannels show decrease in heat transfer coefficients with increasing the heat flux and vapor quality. It can be seen that The maximum heat transfer coefficient in the semi-open microchannels is 1.4 times that of the straight microchannels at the same experimental conditions. The heat transfer enhancement is significant. However, it seems that the effects of mass fluxes on the flow boiling heat transfer coefficients are little for both types of microchannels in the present study. In the meantime, the semi-open microchannels stack with a new influence on the function of flow boiling heat transfer. The phenomenon was also observed in Balasubramanian et al. [31].

Analysis of the Flow Boiling Heat Transfer Mechanisms Based on Observed Flow Patterns

Flow boiling heat transfer mechanisms are intrinsically related to flow patterns and therefore, it is essential to relate the heat transfer mechanisms to the corresponding flow patterns [32]. In the present study, different behaviors above of flow boiling heat transfer of the two types are linked to the type effects on the flow patterns. As mentioned in the forging, the nucleate boiling mechanism dominated the microchannels at the beginning of boiling. Figures 13(a) and (b) show the observed flow patterns in the semi-open micorchannels and the straight microchannels, respectively. As shown in Fig. 13(a), in the semi-open microchannels, the bubbles

bocome bigger and coalesce with each other, because of enough space. It thus delays the transition from bubbly flow to elongated flow. As shown in Fig. 13(b), in the straight microchannels, the expansion of bubbles is restricted by the side walls, thus the size of bubbles are confined to a small limit.

Fig. 14(a) shows the process of elongation bubble's expansion from upstream to downstream at the mass flux of 11.28 kg/m^{2}s and the heat flux of 29.54 kW/m^2 in the semi-open microchannels. At the beginning of the elongation of bubble, it expands in upstream and downstream synchronously because of the wall surface. However, when the fins are stepped down in the downstream, the back-ends of bubbles have more spaces to expand. At the same time, the front-ends of bubbles slow down the speed of expansion towards upstream, as showed in Fig. 14(a) (5-30 ms). As the back-end of bubble coalesces with an adjacent bubble which is in the downstream, the front-end of bubble stops to grow up as showed in Fig. 14(a) (30-40 ms), and with the development of coalescence of two bubbles, the front-end of bubble migrated downstream relatively rapidly until the total integration of both bubbles, as showed in Fig. 14(a) (50-95 ms). According to these observations, the semi-open microchannels effectively prevent the inverse flow in the microchannels and slow down the transition from the bubbly flow to the elongated flow or the churn flow, making the bubbly flow exist in a longer time interval, and thus increasing flow boiling heat transfer performance.

Fig. 14(b) shows the process of elongation of the bubble's expansion from the upstream to the downstream at the mass flux of 11.28 kg/m^{2}s and the heat flux of 9.54 kW/m^2 in the straight microchannels. It can be seen that the flow pattern has been transited to the elongated flow. A transition from the bubbly flow to the elongated flow is much faster than that in the semi-open microchannels due to its more intense wall confinement. In Fig. 14(b) (0-50 ms), the elongation bubbles expand in the upstream and downstream fleetly, and push the upstream bubbles which coalesced together to flow inversely. Due to the increases of the inlet pressure, the elongation bubbles are pushed to the downstream, as shown in Fig. 14(b) (75-00 ms). The period is about 100 ms. The elongated flow pattern and the churn flow pattern in the straight microchannels suppress the nucleate boiling significantly, thus decreasing the flow boiling heat transfer performance as compared to the observed phenomena in the semi-open microchannels.

As showed in Fig. 15(a) and (b), at higher heat fluxes, dry-out and inverted annular flow can be observed in the microchannels at middle and low mass fluxes. This flow patterns result in a serious deterioration of flow boiling heat transfer performance, the heat transfer coefficients decrease sharply, as showed in Figs. 11 and 12. Such flow patterns in microchannels were also reported in other studies. [33, 34].

CONCLUSIONS

In the present study, experiments of flow boiling in a novel structure of microchannels-semi-open microchannels were conducted at different conditions. The effects of heat flux, mass flux, inlet temperature and the microchannel types on the boiling performance were examined. The following conclusions may be obtained from this study.

1. The semi-open microchannels may make the ONB at a smaller wall temperature overshoot than the straight microchannels at the same mass flux. The main reason is because the semi-open microchannels may enhance the number of active nucleate sites, promote the bubble embryos to grow and depart at low wall temperature overshoot.

2. The local flow boiling heat transfer coefficients are dependent on the heat flux, the mass flux and the inlet temperature. The maximum heat transfer coefficients may be achieved at the heat flux of ONB, high mass flux and low inlet temperature.

3. The semi-open microchannels have higher heat transfer behaviors than the straight microchannels. The heat transfer mechanisms are strongly related to the observed flow patterns.

ACKNOWLEDGEMENTS

The authors acknowledge the support by the National Natural Science Foundation of China (No. 51576005).

REFERENCES

[1] Tuckerman, D. B. and Pease, R. F. W., High-Performance Heat Sinking for VLSI, *IEEE Electron Device Lett*, vol. 2, no. 5, pp. 126-129, 1981.

[2] Mudawar, I., Assessment of High-Heat-Flux Thermal Management Schemes, *IEEE Trans. Component Packaging Technol*, vol. 24, no. 2, pp. 141-122, 2001.

[3] Kandlikar, S. G., Steinke, M. E., Tian, S. and Campbell, L. A., High Speed Photographic Observation of Flow Boiling of Water in Parallel Minichannels. *ASME National Heat Transfer Conference, Los Angeles, CA*, 2001, June 10-12.

[4] Steinke, M. E. and Kandlikar, S. G., An Experimental Investigation of Flow Boiling Characteristics of Water in Parallel Microchannels, *Journal of Heat Transfer*, vol. 126, no. 4, pp. 518-526, 2004.

[5] Qu, W. and Mudawar, I., Measurement and Prediction of Pressure Drop in Two-Phase Micro-channel heat sinks, *International Journal of Heat Mass Transfer*, vol. 46, no. 15, pp. 2737-2753, 2003.

[6] Shah, M. M., Unified Correlation for Heat Transfer during Boiling in Plain Mini/Micro and Conventional Channels, *International Journal of Refrigeration*, vol. 74, pp. 606-626, 2017.

[7] Huang, H. X. and Thome, J. R., Local Measurements and A New Flow Pattern Based Model for Subcooled and Saturated Flow Boiling Heat Transfer in

Multi-Microchannel Evaporators, *International Journal of Heat Mass Transfer*, vol. 103, pp. 701-714, 2016.

[8] Cheng, L., Fundamental Issues of Critical Heat Flux Phenomena During Flow Boiling in Microscale-Channels and Nucleate Pool Boiling in Confined Spaces, *Heat Transfer Engineering*, vol. 34, no. 13, pp. 1016-1043, 2013.

[9] Wu, H. Y. and Cheng, P., Boiling Instability in Parallel Silicon Microchannel Sat Different Heat Flux, *International Journal of Heat Mass Transfer*, vol. 47, no. 17–18, pp. 3631-3641, 2004.

[10] Hetsroni, G., Mosyak, A., Pogrebnyak, E. and Segal, Z., Explosive Boiling of Water in Parallel Micro-channels, *International Journal Multiphase Flow*, vol. 31, no. 4, pp. 371-392, 2005.

[11] Chen, C. A., Chang, W. R., Li, K. W., Lie, Y. M. and Lin, T. F, Subcooled Flow Boiling Heat Transfer of R-407 and Associated Bubble Characteristics in Narrow Annular Duct, *International Journal of Heat Mass Transfer*, vol. 52, nos. 13-14, pp. 3147-3158, 2009.

[12] Zhang, C. B., Chen, Y. P. and Wu, R, Flow Boiling in Constructal Tree-shaped Minichannel Network, *International Journal of Heat and Mass Transfer*, vol. 54, no. 1-3, pp. 202-209, 2011.

[13] Chen, Y. P. and Cheng, P., Heat Transfer and Pressure Drop in Fractal Tree-like Microchannel Nets, *International Journal of Heat and Mass Transfer*, vol. 45, no. 13, pp. 2643-2648, 2002.

[14] Wu, H. Y. and Cheng, P. Visualization and Measurements of Periodic Boiling in Silicon Microchannels, *International Journal of Heat and Mass Transfer*, vol. 46, no. 14, pp. 2603- 2614, 2003.

[15] Wu, H. Y. and Cheng, P., Liquid/Two-phase/Vapor Alternating Flow During Boiling in Microchannels at High Heat Flux, *International Communications in Heat and Mass Transfer*, vol. 30, no. 3, pp. 295-302, 2003.

[16] Wang, H. L., Wu, H. C., Wang, S. K., Hung, T. C. and Ruey, J. Y., A Study of Mini-channel Thermal Module Design for Achieving High stability and High Capability in Electronic Cooling, *Applied Thermal Engineering*, vol. 51, nos. 1-2, pp. 1144-1153, 2013.

[17] Yang, F., Dai, X., Kuo, Ch. J., Peles, Y., Khan, J. and Li, C., Enhanced Flow Boiling in Microchannels by Self-sustained High Frequency Two-phase Oscillations, *International Journal of Heat and Mass Transfer*, vol. 58, nos. 1-2, pp. 402-412, 2013.

[18] Kandlikar, S. G., Theodore, W., Ankit, K. and Valentina, M., Enhanced Flow Boiling over Open Microchannels with Uniform and Tapered Gap Manifolds, *Journal of Heat Transfer*, vol. 135, no. 6, 061401 (9 pages), 2013.

[19] Cheng, L. and Xia, G., Fundamental Issues, Mechanisms and Models of Flow Boiling Heat Transfer in Microscale Channels, *International Journal of Heat and Mass Transfer*, vol. 108, Part A, pp. 97-127, 2017.

[20] Ma, P., Xia, S. and Xia, Q., Concise Handbook of Chemical Property Data. Beijing, China: Chemical Industry Press, 2013.

[21] Taylor, J. R., An Introduction to Error Analysis, *second ed, University Science Books*, 1997.

[22] Galvis, E and Culham, R., Measurements and Flow Pattern Visualizations of Two-phase Flow Boiling in Single Channel Microevaporators, *International Journal of Multiphase Flow*, vol. 42, pp. 52-61, 2012.

[23] Sun, Y., Zhang, L., Xu, H. and Zhong, X., Flow Boiling Enhancement of FC-72 from Microporous Surfaces in Minichannels, *Experimental Thermal and Fluid Science*, vol. 35, no. 7, pp. 1418–1426, 2011.

[24] Steinke, M. E. and Kandlikar, S. G., An Experimental Investigation of Flow Boiling Characteristics of Water in Parallel Microchannels, *Journal of Heat Transfer*, vol. 126, no. 4, pp. 518–526, 2004.

[25] Agostini, B., Thome, J. R., Fabbri, M., Michel, B., Calmi, D. and Kloter, U., High Heat Flux Flow Boiling in Silicon Multi-microchannels - Part I: Heat Transfer Characteristics of Refrigerant R236fa, *International Journal of Heat and Mass Transfer*, vol. 51, nos. 21-22, pp. 5400-5414, 2008.

[26] Agostini, B., Thome, J. R., Fabbri, M., Michel, B., Calmi, D. and Kloter, U., High Heat Flux Flow Boiling in Silicon Multi-microchannels - Part II: Heat Transfer Characteristics of Refrigerant R245fa, *International Journal of Heat and Mass Transfer*, vol. 51, nos. 21-22, pp. 5415-5425, 2008.

[27] Sumith, B., Kaminaga, F. and Matsumura, K., Saturated Flow Boiling of Water in a Vertical Small Diameter Tube, *Experimental Thermal and Fluid Science*, vol. 27, no. 7, pp. 789-801, 2003.

[28] In, S. and Jeong, S., Flow Boiling Heat Transfer Characteristics of R123 and R134a in a Micro-channel, *International Journal of Multiphase Flow*, vol. 35, no. 11, pp. 987–1000, 2009.

[29] Xu, J. L., Shen, S., Gan, Y. H., Zhang, W. and Su, Q. C., Transient Flow Pattern Based Microscale Boiling Heat Transfer Mechanisms, *Journal of Micromechanics and Microengineering*, vol. 15, no. 6, pp. 1344-1361, 2005.

[30] Bao, Z. Y., Fletcher, D. F. and Haynes, B. S., Flow Boiling Heat Transfer of Freon R11 and HCFC123 in Narrow Passages, *International Journal of Heat and Mass Transfer*, vol. 43, no. 18, pp. 3347-3358, 2000.

[31] Balasubramanian, K., Lee, P. S., Teo, C. J. and Chou, S. K., Flow Boiling Heat Transfer and Pressure Drop in Stepped Fin Microchannels, *International Journal of Heat and Mass Transfer*, vol. 67, pp. 234–252, 2013.

[32] Cheng, L, Ribatski, G. and Thome, J. R., Two Phase Flow Patterns and Glow Pattern Maps: Fundamentals and Applications, *Applied Mechanics Reviews*, vol. 61,no. 5, pp. 050802-1- 050802-28, 2008.

[33] Kalani, A. and Kandlikar, S. G., Flow Patterns and Heat Transfer Mechanisms during Flow Boiling over Open Microchannels in Tapered Manifold (OMM), *International Journal of Heat and Mass Transfer*, vol. 89, pp. 494–504, 2015.

[34] Deng, D., Chen, R., He, H., Feng, J., Tang, Y. and Zhou, W., Effects of Heat Flux, Mass Flux and Channel Size on Flow Boiling Performance of Reentrant Porous Microchannels, *Experimental Thermal and Fluid Science*, vol. 64, pp. 13–22, 2015.

Table 1 Properties of acetone and water tested at saturation temperature [20].

Property	Unit	Acetone	Water
Pressure	kPa	101.325	101.325
Liquid density	kg/m^3	788	958
Vapor density	kg/m^3	2	0.6
constant pressure specific heat	kJ/kg·K	2.253	4.220
Latent heat	kJ/kg	498	2257
Liquid thermal conductivity	W/m·K	0.1521	0.683
Liquid dynamic viscosity	μPa·s	236.2	282.5
Vapor dynamic viscosity	μPa·s	8.248	12.023
Surface tension	N/m	0.0198	0.0589

Table 2 Uncertainties of the experimental parameters.

Parameters	Uncertainty
Temperature (T)	±0.1°C
Total area effective for convection (A_{ch})	±0.36%
Flow boiling heat transfer coefficient ($h_{tp,tci}$)	±0.8%
Mass flow rate ($\dot{m}$)	±0.02%
Effective heat adsorption (q_{eff})	±0.5%
Vapor quality (x)	±0.5%

Fig. 1 Schematic of the experimental loop.

Fig.2 Geometries of the microchannel heat sinks: (a) the heat sink with 19 straight microchannels; (b) the heat sink with 19 semi-open microchannels.

Fig. 3 Schematic of the test section: (a) Exploded view drawing; (b) Sectional view drawing.

Fig. 4 Heat transfer modes: (a) the straight microchannels; (b) the semi-open microchannels.

Fig. 5 The boiling curves of straight microchannels: (a) at high mass flux, (b) at low mass flux.

Fig. 6 The boiling curves of semi-open microchannels: (a) at high mass flux, (b) at low mass flux.

Fig. 7 The effect of the heat flux and the mass flux on flow boiling heat transfer coefficient with respect to the effective heat flux.

Fig. 8 The effect of the heat flux and the mass flux on flow boiling heat transfer coefficient with respect to the vapor quality.

Fig. 9 The effect of the inlet temperature on the flow boiling heat transfer coefficient with respect to the effective heat flux.

Fig. 10 The effect of the inlet temperature on flow boiling heat transfer coefficient with respect to the vapor quality.

Fig. 11 The effect of the microchannels types on the flow boiling heat transfer coefficient with respect to the effective heat flux.

Fig. 12 The effect of the microchannel types on flow boiling heat transfer coefficient with respect to the vapor quality.

Fig 13 Observed bubbly flow in microchannels: (a) semi-open microchannels; (b) straight microchannels.

Fig. 14. (a) bubble elongation of semi-open microchannels at Tin = 20 ℃, G = 11.28 kg/m^{2}s and q"eff = 29.54 kW/m2; (b) bubble elongation of straight microchannels at T_{in} = 20 ℃, G = 11.28 kg/m^{2}s and q"eff = 29.54 kW/m^2.

Fig. 15. Flow patterns for semi-open microchannels (a) Dry-out at T_{in} = 20 ℃, G = 11.28 kg/m^{2}s and q"eff = 72.81 kW/m^2, (b) Inverted annular flow at T_{in} =20℃, G = 6.94 kg/m^{2}s and q"eff = 58.85 kW/m^2.

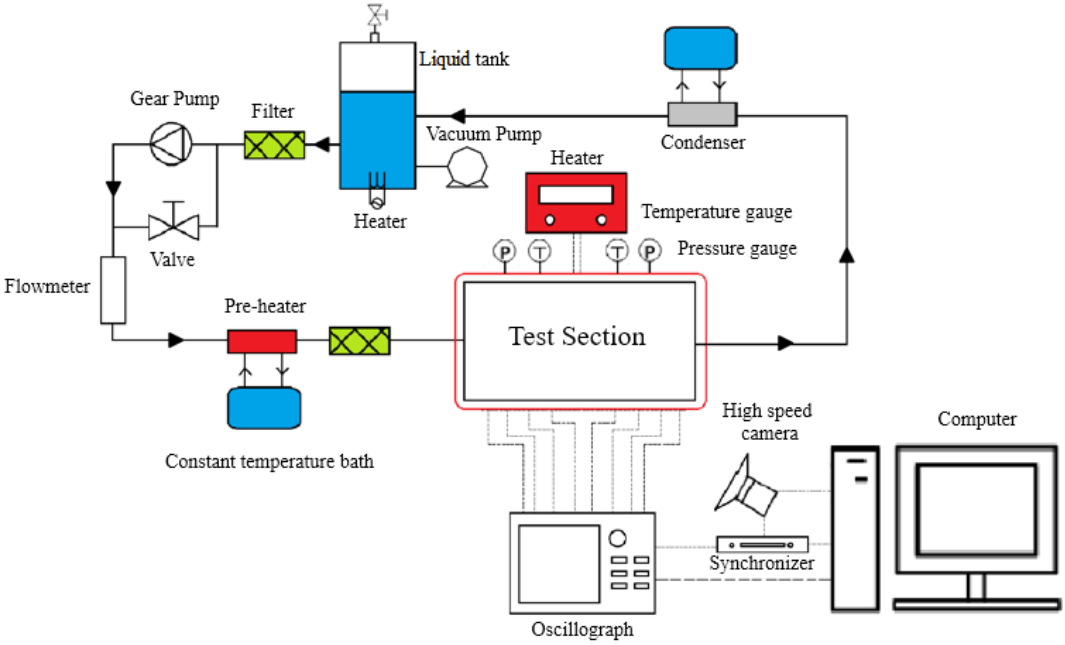

Fig. 1 Schematic of the experimental loop.

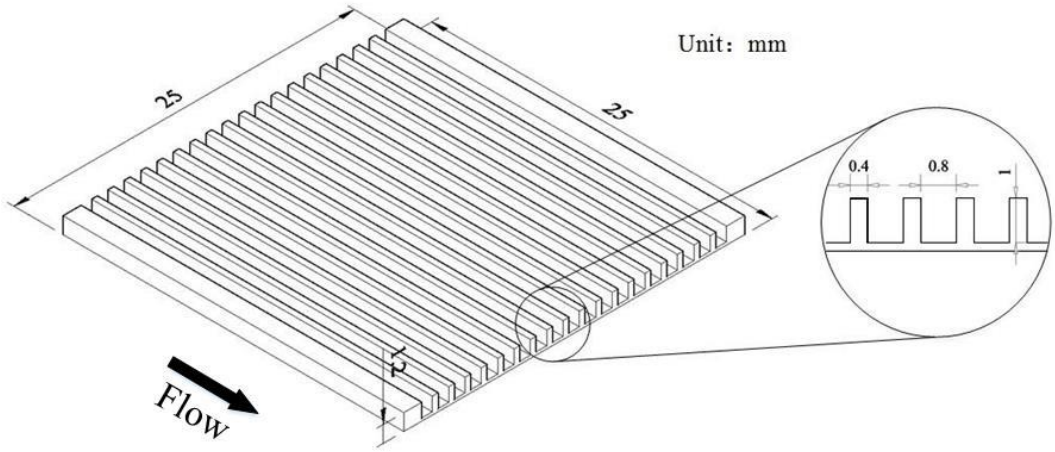

(a)

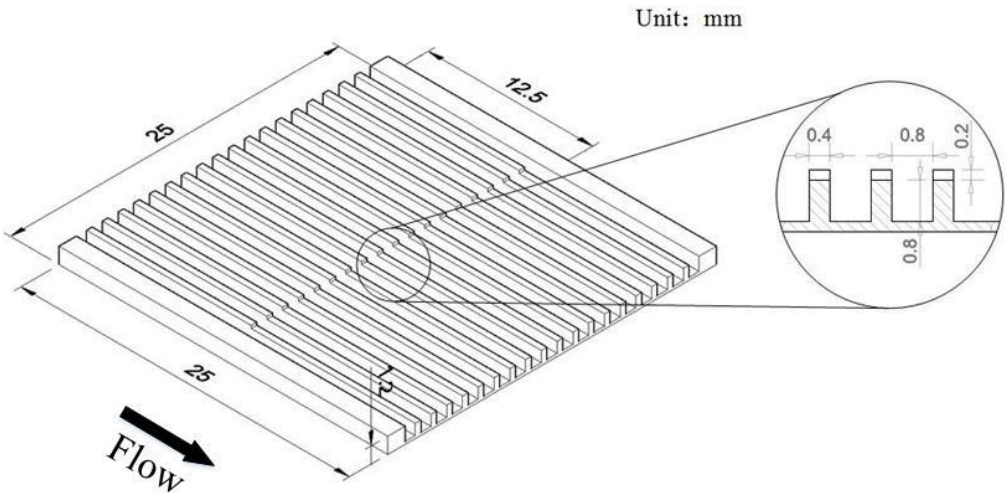

(b)

Fig.2 Geometries of the microchannel heat sinks: (a) the heat sink with 19 straight microchannels; (b) the heat sink with 19 semi-open microchannels.

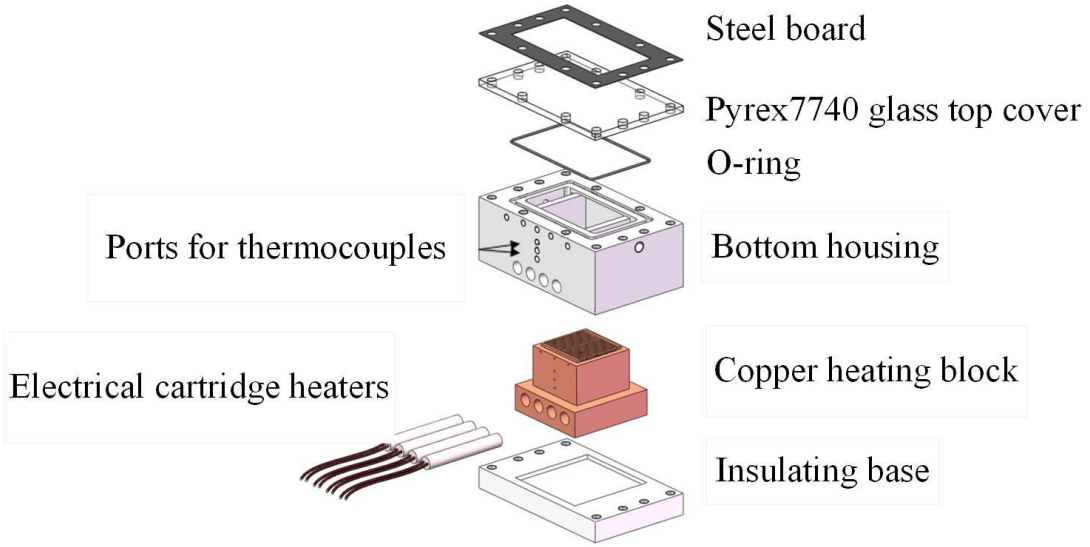

(a)

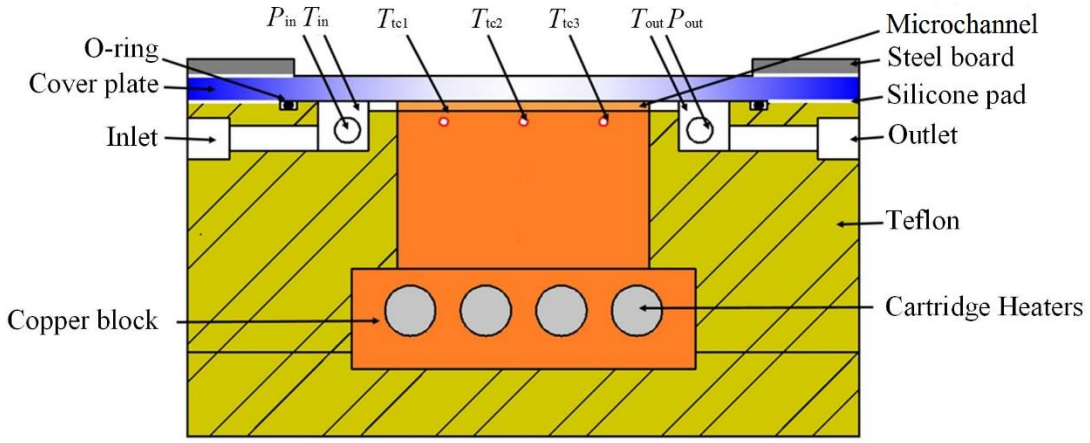

(b)

Fig. 3 Schematic of the test section: (a) Exploded view drawing; (b) Sectional view drawing.

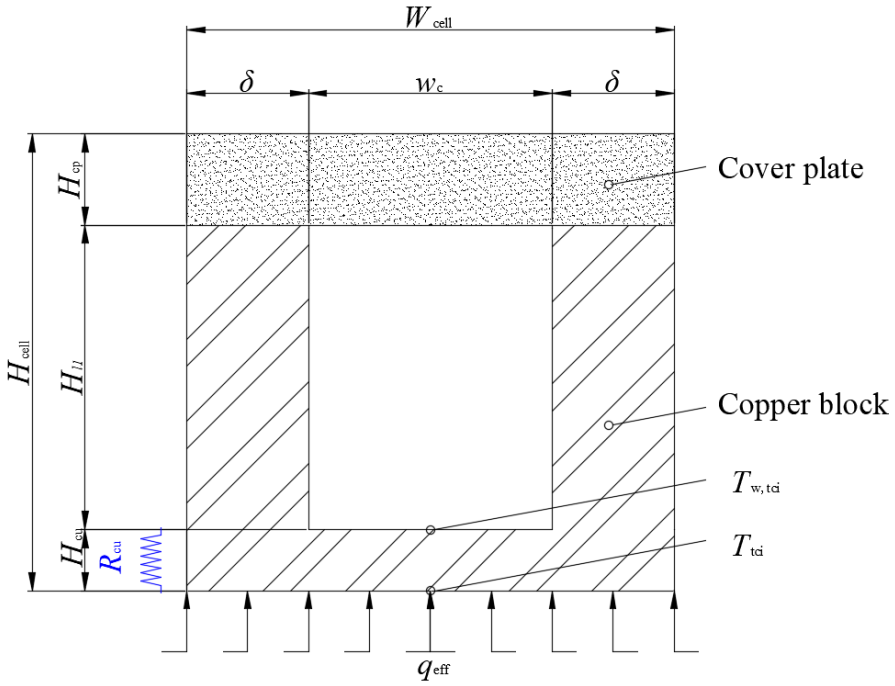
W_{cell}
δ
w_c
δ
H_{cp}
Cover plate
H_{cell}
H_{ll}
Copper block
$T_{w,tci}$
H_{cu}
R_{cu}
T_{tci}
q_{eff}

(a)

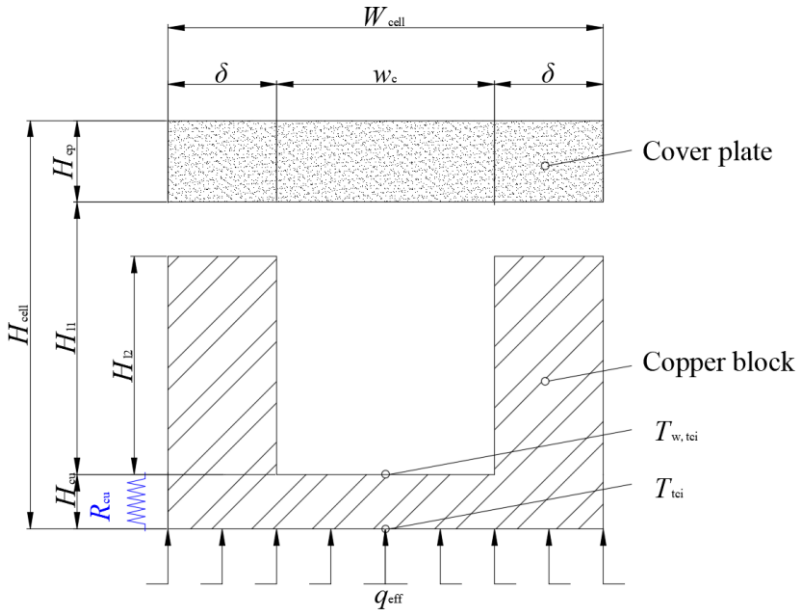

(b)

Fig. 4 Heat trandfer modes: (a) the straight microchannels; (b) the semi-open microchannels.

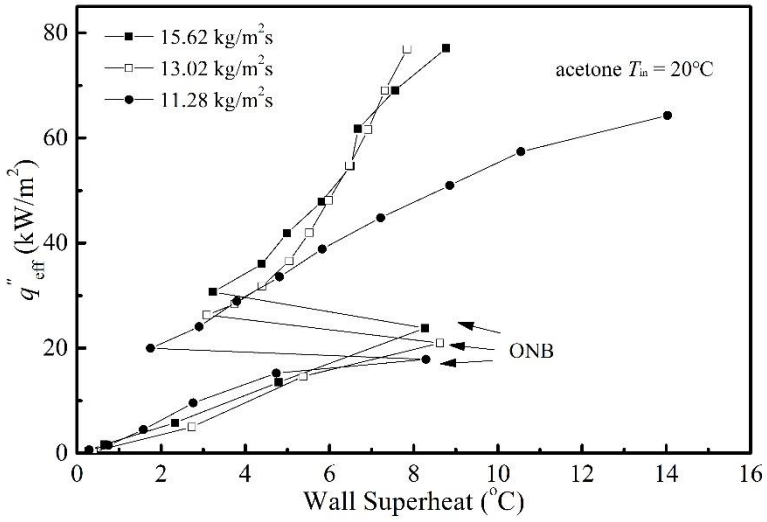

(a)

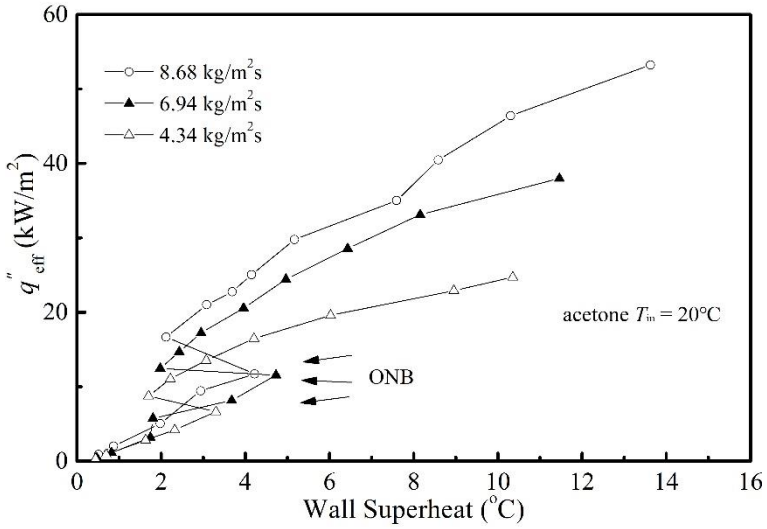

(b)

Fig. 5 The boiling curves of straight microchannels: (a) at high mass fluxes, (b) at low mass fluxes.

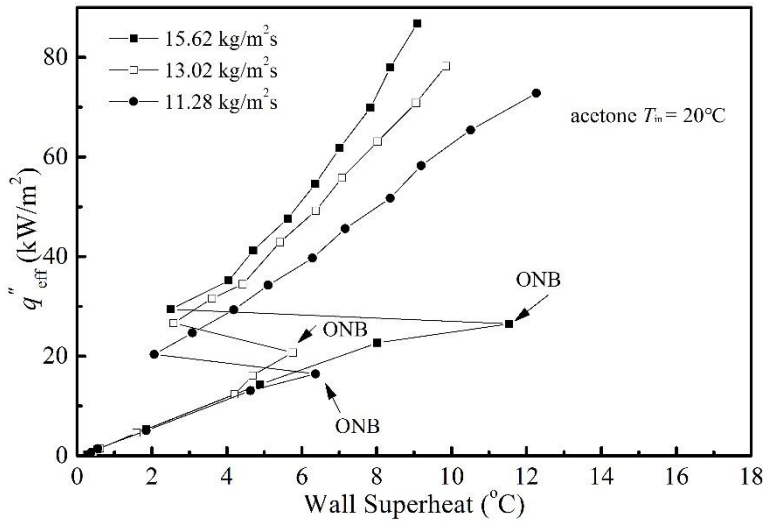

(a)

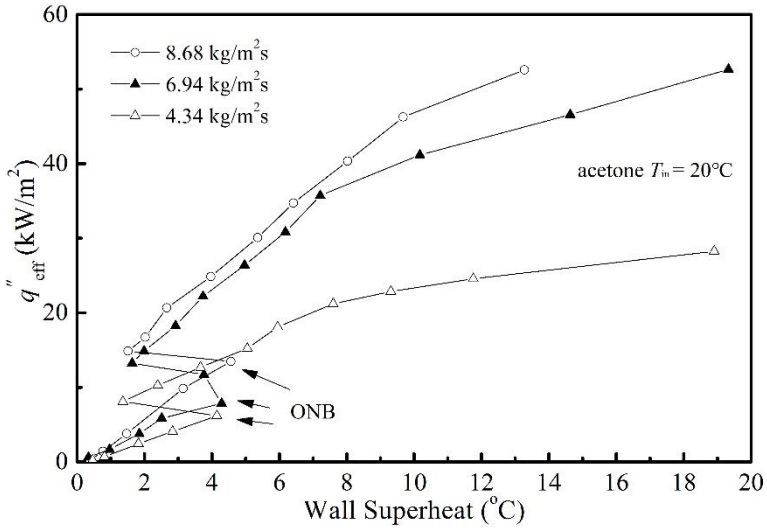

(b)

Fig. 6 The boiling curves of semi-open microchannels: (a) at high mass fluxes, (b) at low mass fluxes.

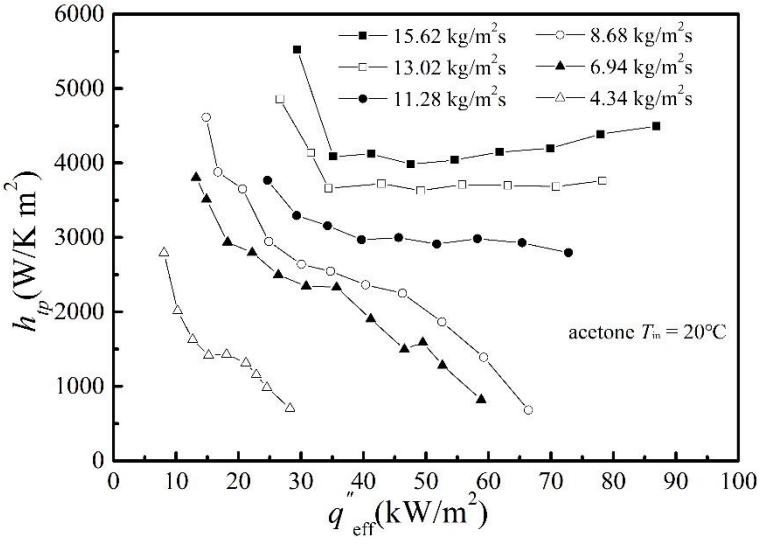

Fig. 7 The effect of the heat flux and the mass flux on flow boiling heat transfer cofficient with respect to the effective heat flux.

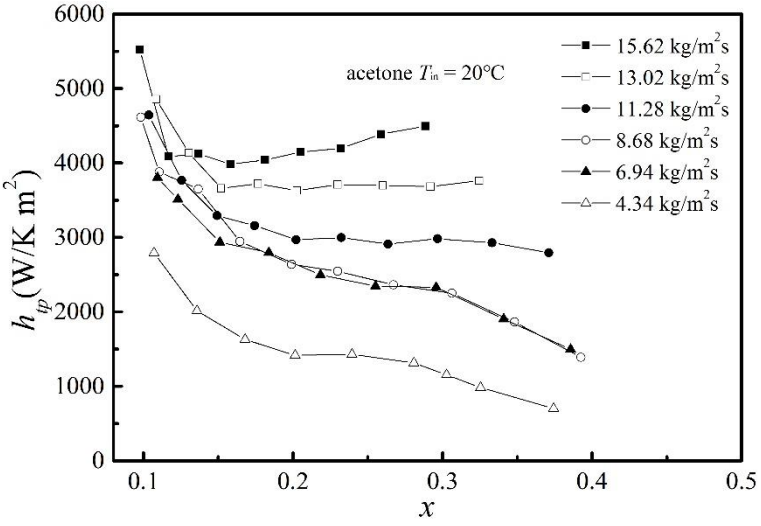

Fig. 8 The effect of the heat flux and the mass flux on flow boiling heat transfer cofficient with respect to the vapor quality.

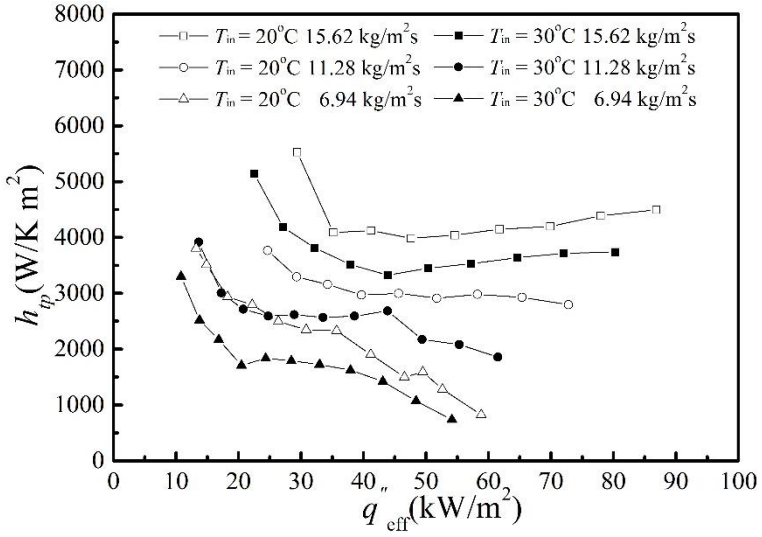

Fig. 9 The fffect of the inlet temperature on flow boiling heat transfer cofficient with respect to the effective heat flux.

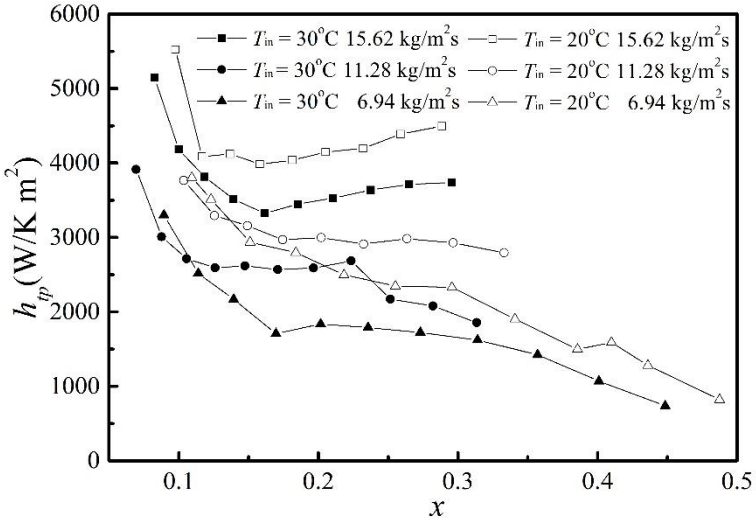

Fig. 10 The effect of the inlet temperature on flow boiling heat transfer cofficient with respect to the vapor quality.

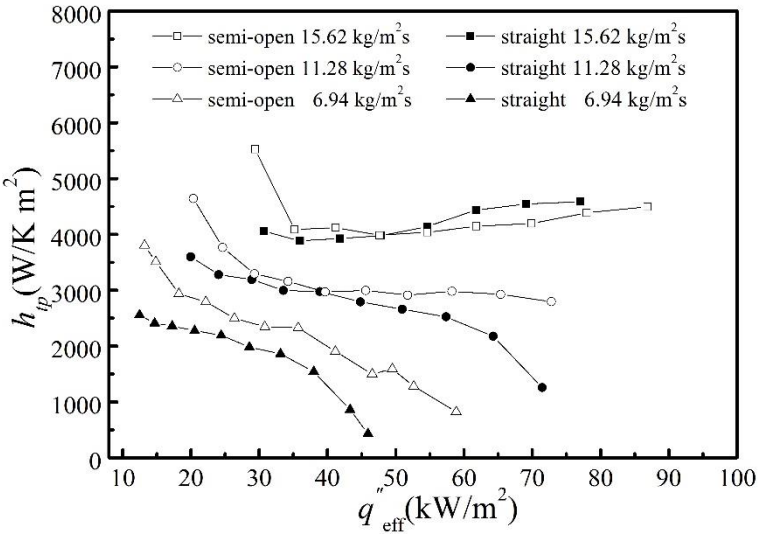

Fig. 11 The Effect of microchannel types on flow boiling heat transfer cofficient with respect to the effective heat flux.

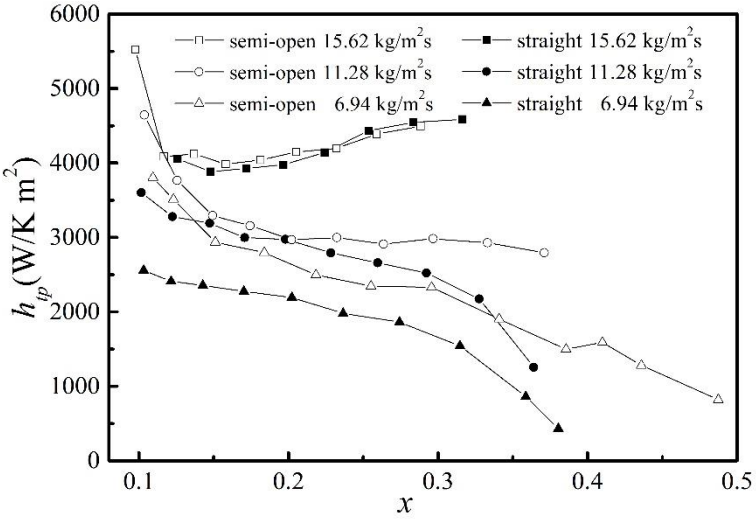

Fig. 12 The effect of microchannel types on flow boiling heat transfer cofficient with respect to the vapor quality.

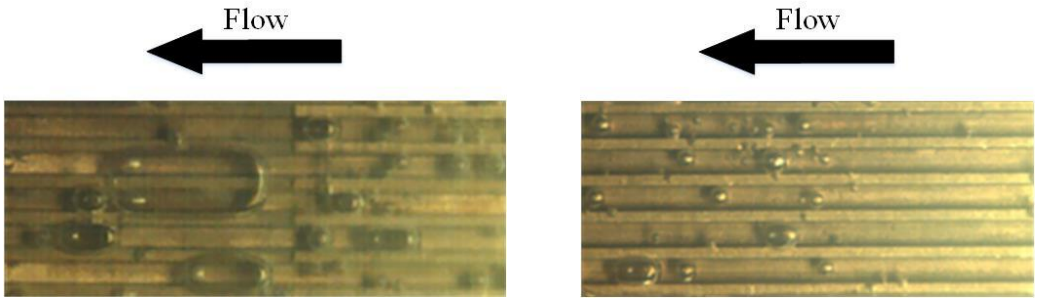

(a) (b)

Fig 13 Bubbly flow in microchannels: (a) semi-open microchannels; (b) straight microchannels.

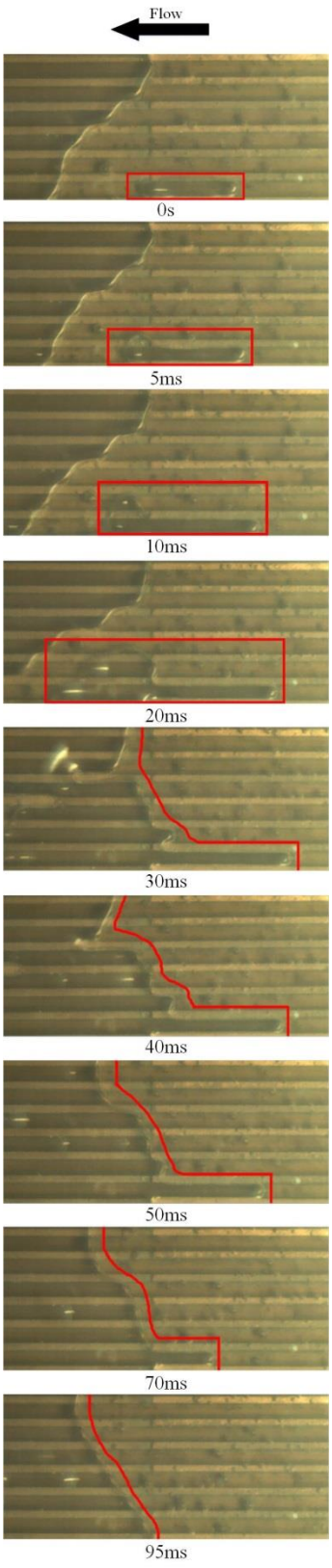
Flow
0s
5ms
10ms
20ms
30ms
40ms
50ms
70ms
95ms

(a)

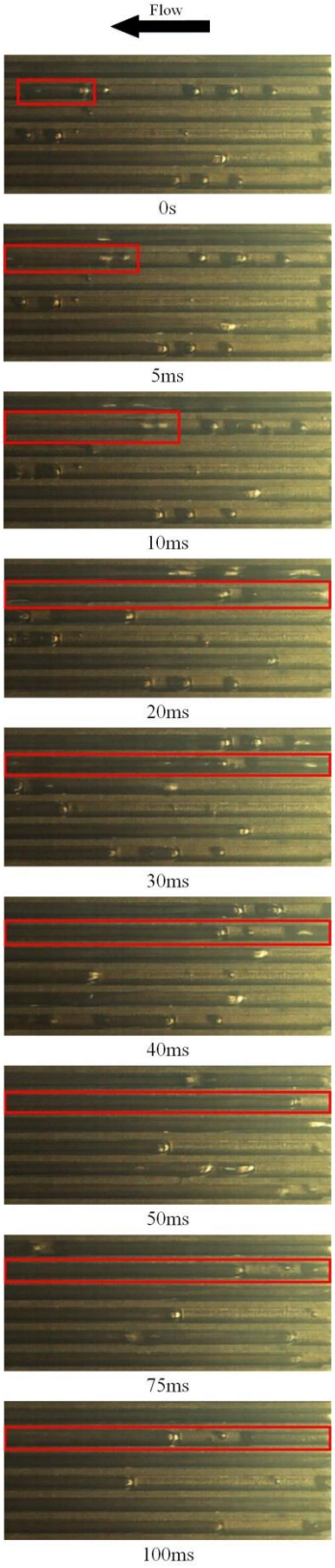
Flow
0s
5ms
10ms
20ms
30ms
40ms
50ms
75ms
100ms

(b)

Fig. 14. (a) bubble elongation of semi-open microchannels at Tin = 20 ℃, G = 11.28 kg/m^{2}s and q"eff = 29.54 kW/m2; (b) bubble elongation of straight microchannels at T_{in} = 20 ℃, G = 11.28 kg/m^{2}s and q"eff = 29.54 kW/m^2.

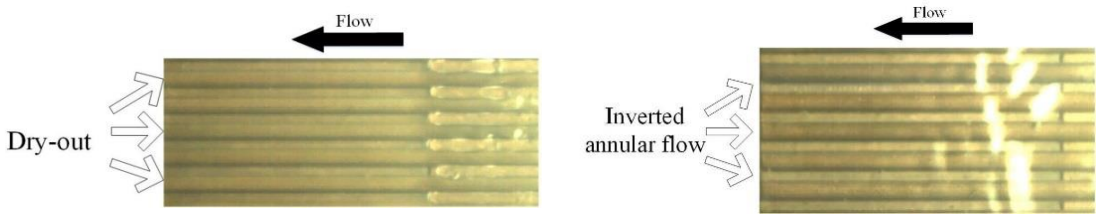

(a) (b)

Fig. 15. Flow patterns for semi-open microchannels (a) Dry-out at T_{in} = 20 ℃, G = 11.28 kg/m^{2}s and q"eff = 72.81 kW/m^2, (b) Inverted annular flow at T_{in} =20℃, G = 6.94 kg/m^{2}s and q"eff = 58.85 kW/m^2.

Notes on Contributors

Guodong Xia is a leading professor in Thermal Energy Engineering at Beijing University of Technology, China. He received his Ph.D. in Thermal Energy Engineering at the State Key Laboratory of Multiphase Flow at Xi'an Jiaotong University, China in 1996. He was a visiting professor in the Institute of Process Engineering at the University of Hanover, Germany in 2000-2001. His research interests include fundamentals and applications of microscale heat transfer, multiphase flow and heat transfer, waste energy recovery, thermal energy system, heat exchanger design and enhanced heat transfer. He is a member of the multiphase flow committee of the Chinese Society of Engineering Thermophysics and a member of the multiphase flow committee of the Chinese Society of Theoretical and Applied Mechanics. He has published more than 100 papers in journals and conferences.

Yue Cheng is currently working on a postgraduate program at the College of Environmental and Energy Engineering, Beijing University of Technology, Chaoyang, Beijing, China. He is working in flow pattern, pressure drop and boiling heat transfer in microchannel. He obtained his B.E. in 2014 from Beijing University of Technology, China.

Lixin Cheng is a principal lecturer at Sheffield Hallam University, UK. He obtained his Ph.D. in Thermal Energy Engineering at the State Key Laboratory of Multiphase Flow at Xi'an Jiaotong University, China in 1998. He has extensive international working and collaboration experience as associate professor, senior lecturer, lecturer and research fellows at Aarhus University, University of Portsmouth, University of Aberdeen, Swiss Federal Institute of Technology (EPFL), Leibniz University of Hannover, London South Bank University and Eindhoven University of Technology for 18 years. He was awarded an Alexander von Humboldt Research Fellowship in 2004-2006. His research interests include multiphase flow and heat transfer, nanofluid two-phase flow and heat transfer and compact and micro-heat exchangers. He has published more than 100 papers in journals and conferences, 10 book chapters and edited 10 books. He has been an associate editor of *Heat Transfer Engineering* since 2016.

Yifan Li is currently a Ph.D. candidate at the College of Environmental and Energy Engineering, Beijing University of Technology, Chaoyang, Beijing, China. She is mainly engaged in the fields of microelectronic cooling, fluid flow and heat transfer in micro-scale, especially for the complicated microchannels.